from "Clinical Dosimetry Measurements in Radiotherapy", eds D.W.O. Rogers and J.E. Cygler
Medical Physics Publishing (Madison WI) 2009

Chapter 5

Monte Carlo Applications in Measurement Dosimetry

J. Seuntjens, Ph.D.,[1] and D.W.O. Rogers, Ph.D.[2]
[1]Medical Physics Unit, McGill University
Montreal General Hospital
Montreal, Quebec, Canada
[2]Carleton Laboratory for Radiotherapy Physics
Carleton University, Ottawa, Ontario, Canada

1. Introduction

In recent years, the use of Monte Carlo techniques in radiation therapy has become widespread. Applications include treatment source simulations (accelerators, radioactive sources) along with sophisticated dynamic beam modifiers, imaging panel simulations (flat panel imagers, cone beam CT), diagnostic and treatment planning imaging equipment simulations (CT, simulators, kV machines), and treatment planning dose calculations. Monte Carlo techniques have been equally important in shielding applications and new treatment device development such as, for example, the Gamma Knife® Perfexion™ . The reader is invited to consult the many reviews covering specific aspects of Monte Carlo (MC) techniques in radiation therapy.

Monte Carlo techniques have been the basis for the improved understanding of detector response for radiation therapy. This, however, required considerable research in electron transport algorithms, multiple scattering theory, boundary crossing algorithms, cross sections, etc. Consistent and accurate detector response calculations required significant developments of the condensed history Monte Carlo codes over the last two decades. But in the end, it was through detector response calculations for primary standards in standards laboratories that the significant accuracy improvements required for clinical measurement dosimetry have been realized. The impact of consistent and rigorous detector response calculations had consequences on the role of Monte Carlo techniques in radiation therapy far beyond the use of ionization chambers or other detectors. Firstly, accurate calculation of dose ratios, as needed in detector response calculations, are also important in other areas such as treatment planning, as pointed out in chapter 3. Secondly, rigorous calculations of transport across boundaries and accurate energy loss evaluation had impact in all of the above-mentioned applications of MC to radiation therapy. So it is reasonable to say that improvements have, along with ingenious speed-up techniques, rendered Monte Carlo techniques an enormously powerful tool in radiation therapy applications.

This chapter concentrates on the application of Monte Carlo techniques in measurement dosimetry along different stages of the dosimetry chain including primary standards for air kerma and absorbed dose as well as in clinical reference dosimetry of open and complex beams. We discuss the central role that Monte Carlo techniques have played in supporting and extending basic cavity theory to radiation standards and clinical measurement dosimetry.

The chapter will mainly concentrate on ionization chambers, although some other detectors will also be mentioned in the context of applications in relative dosimetry.

2. The Context of Chamber Response: Cavity Theory

Chapter 3 discusses in detail the cavity theory basis for measurement dosimetry and the conditions that must be fulfilled to make cavity theory accurate. Chapter 4 presents a consistent notation that separates the intrinsic energy dependence from

the dosimetric (absorbed dose or air kerma) energy dependence. We will base the notation used in the present chapter on that nomenclature.

Starting from equation (4.17), which describes under favorable but still fairly general conditions, the relation between a corrected detector signal and the dose to the medium, or air kerma:

$$D_{med}(Q) \text{ or } K_{air}(Q) = f(Q) k_{bq}(Q) k_l M_{\text{det}}(Q, D, \dot{D}, \theta, \phi), \tag{5.1}$$

where the product $f(Q)k_{bq}(Q)k_l$ represents the detector absorbed-dose or air-kerma calibration coefficient. The factor k_{bq} expresses the beam quality [or linear energy transfer (LET)] dependence of the dose to the detector per unit corrected reading. The coefficient k_l accounts for any detector nonlinearity as a function of total dose, which is nonexistent for an ion chamber and thus unity. The factor $f(Q)$ accounts for the beam quality dependence of the absorbed dose or kerma in the medium of interest per unit absorbed dose in the detector. For air-filled ionization chambers, k_{bq} is a constant which has traditionally been termed N_{gas} (in TG-21 nomenclature, AAPM TG–21 1983) or $N_{D,air}$ (in TRS-277 nomenclature, IAEA 1987) and can be written as:

$$k_{bq}(Q) = \left(\frac{W}{e}\right)_{air} \frac{1}{m_{air}} \equiv N_{gas} \equiv N_{D,air}. \tag{5.2}$$

The absorbed-dose energy dependence for measurement in a phantom is described by the factor $f(Q)$ and is conventionally calculated using Spencer-Attix cavity theory, with correction factors, factorized as:

$$f(Q) = \left(\frac{\bar{L}}{\rho}\right)_{air}^{med} P_{repl} P_{wall} P_{stem} P_{cel}, \tag{5.3}$$

where $\left(\bar{L}/\rho\right)_{air}^{med}$ represents the average restricted collision stopping-power ratio, medium to air and the P-factors corrections for replacement, wall composition, stem effects, and air central electrode effects, respectively.

The air-kerma energy dependence takes the form:

$$f(Q) = \frac{1}{1 - g_{air}} \left(\frac{\bar{L}}{\rho}\right)_{air}^{wall} \left(\frac{\overline{\mu_{en}}}{\rho}\right)_{wall}^{air} K_{wall} K, \tag{5.4}$$

where the ratio $\left(\bar{L}/\rho\right)_{air}^{wall}$ is the average restricted collision stopping-power ratio, wall to air averaged over the secondary electron spectrum in the wall, $\left(\overline{\mu_{en}}/\rho\right)_{wall}^{air}$ is the ratio of average mass-energy absorption coefficients air to wall and converts wall collision kerma into collision kerma free in air. The wall correction factor, K_{wall} corrects for the effects of attenuation and scatter on photon and electron

fluence. Additional K factors are introduced to deal with effects such as non-wall material equivalence of the build-up cap, point-source non-uniformity, etc. The leading factor $1/(1 - g_{air})$ converts air collision kerma into air kerma.

The factorization of the energy dependence in ionization chamber dosimetry into smaller correction factors has traditional pragmatic reasons. Firstly, the energy dependence in dose measurements in well-behaved conditions could largely be described by just the restricted stopping-power ratio. For example, for cylindrical chambers in high-energy photon beams, the energy dependence normalized at ^{60}Co (or, in other words, the k_Q factor), can be described to within 1% by just considering restricted stopping-power ratios water to air. The additional corrections bring in some chamber-type dependence that is quite limited. Hence, the majority of the physics of the dose conversion is in the stopping-power ratio and the additional factors represented a limited adjustment to this. In dosimetry protocols of the vintage of TG-51 and TRS-398, for example, stopping-power ratios were Monte Carlo calculated whereas the correction factors were based on a mixture of different methods, including measurements and simple models enhanced by Monte Carlo calculations (see chapter 9).

Monte Carlo techniques have been gradually introduced in measurement dosimetry as a means to calculate quantities for standards and reference dosimetry protocols. Before the capability of consistent absolute detector response calculations existed, Monte Carlo techniques were mainly used to calculate ratios, such as, stopping-power ratios, ratios of doses in situations of differential geometry or material, etc.

With the introduction of Monte Carlo methods to calculate stopping-power ratios and detector correction factors, the order in which the corrections are introduced must be well defined. Obviously, a factorization in a stopping-power ratio along with corrections that are independent from each other is not unique and, in fact, arbitrary. If we denote the average dose to the cavity air in the real chamber as $D_{air}^{w,c,}$ containing "wall," "central electrode," and "stem" as denoted by the superscripts *w, c,* and *s,* respectively. The following identity for D_{air}, the average dose to the air volume in absence of contributions of wall, etc., describes one way the different corrections can be defined consistently:

$$D_{air} = \frac{D_{air}}{D_{air}^{w}} \cdot \frac{D_{air}^{w}}{D_{air}^{w,c}} \cdot \frac{D_{air}^{w,c}}{D_{air}^{w,c,s}} \cdot D_{air}^{w,c,s} = P_{wall} P_{cel} P_{stem} \cdot D_{air}^{w,c,s}, \tag{5.5}$$

where $D_{air}^{w,c,s}$ can be related to the chamber reading, corrected for LET dependencies, air nonlinearities and other dependencies as discussed in chapter 4. The relation between D_{air} and $D_w(z)$ can be expressed as:

$$D_w(z) = D_{air} \cdot \left(\frac{\bar{L}}{\rho}\right)_{air}^{w} P_{repl}. \tag{5.6}$$

The replacement correction factor combines the effect of the changes in electron fluence both in distribution and magnitude and effectively "fixes" the Spencer-Attix

stopping-power ratio for this sometimes drastic effect. The magnitude of the replacement correction depends partially on what has been chosen as the measurement point, e.g., on the chamber axis in the center of the mass of the air volume and, as seen later on in the chapter, this is strongly influenced by the local gradients.

The fact that the replacement correction factor is thus not really distinguishable from the method used in the calculation of the stopping-power ratio is illustrated in figure 5-1. The figure represents the different steps involved in correcting an ionization chamber reading to absorbed-dose to water at a point whereby the replacement correction factor and the stopping-power ratio are not calculated separately and the dose ratio $D_w(z)/D_{air}$(cavity) is just formally represented by the product $\left(\bar{L}/\rho\right)_{air}^{w} P_{repl}$.

The realization of the fact that the stopping-power ratio and perturbation correction factor (product of wall, stem, replacement factors) cannot really be distinguished uniquely leads to important clinical consequences with regard to the applicability of Spencer-Attix restricted stopping-power ratios, especially in conditions that differ from static open fields and conventional reference conditions, and thus severely hamper the Bragg-Gray conditions (see chapter 3). It is sometimes mistakenly thought that to use Bragg-Gray cavity theory charged particle equilibrium (CPE) must exist in the absence of the detector at the point at which the detector will

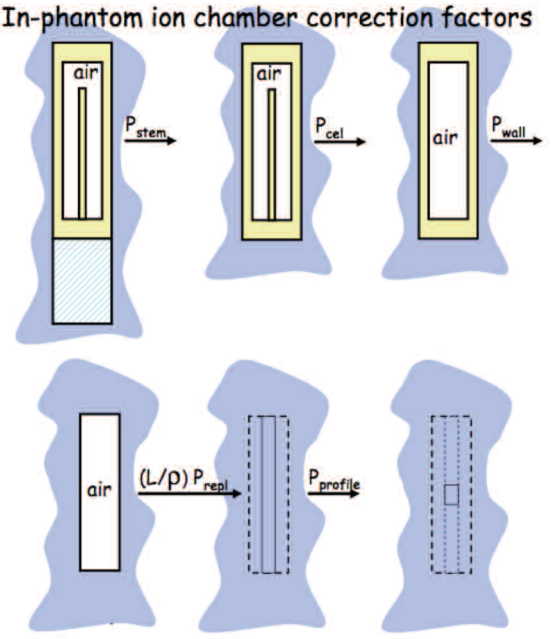

Figure 5-1. Summary of the steps involved in correcting the ionization chamber signal and definition of correction and conversion factors.

be placed. Stopping-power ratios can be calculated in the absence of charged particle equilibrium (they are used extensively in electron beams without any CPE) but their usefulness (i.e., their accuracy as an approximation of the dose ratio) depends on whether the additional effects—most importantly fluence perturbation and gradient effects—are significant. For example, Sanchez-Doblado et al. (2003) demonstrate that Spencer-Attix stopping-power ratios for small fields do not differ from conventional reference fields by more than 0.4%. However, this statement does not make any guarantees about accuracy of narrow-field dosimetry for which these stopping-power ratios are applicable.

3. Calculation Accuracy and the Fano Test

3.1 Condensed History Transport

Monte Carlo methods have been used to predict dose calculations with radiation dosimeters for applications in standards and clinical dosimetry since the late 1970s. There are several problems that hampered, until about a decade ago, the accurate calculation of the response of detectors such as ionization chambers. In brief, these problems had to do with the way detailed electron transport is handled in a Monte Carlo code. Clearly, the large number of Coulomb interactions that an electron undergoes prevents, still today, the explicit simulation of electron transport in an analog way, interaction-by-interaction. In a seminal paper Berger (1963) discussed the condensed history technique for electron transport. Condensed history electron transport takes advantage of the concept of mathematical steps in which the effect of a large number of electron interactions are grouped together (Rogers and Bielajew 1990). In so-called class II algorithms, the step length is primarily determined by the probability distribution for a knock-on (electron-electron coulomb) interaction in which a fairly large amount of energy (up to $T/2$, where T is the kinetic energy) can be transferred. Over the step-length, for a curvature-corrected step, the average energy loss is determined by using the restricted stopping power to account for the effect of soft collisions. The electron direction after completion of a step is determined based on a multiple-scattering theory. All this has to be performed such that, on average, the emerging angular and energy distributions are realistic. Multiple-elastic-scattering theories are developed for transport through single infinite materials. Problems arise, however, when transport involves the crossing of a boundary. The choice of the step-length is then not only based on the probability for the occurrence of an electron-electron interaction but should also be dictated by the proximity of the boundary (or by user determined step control parameters). The practical implementation of this leads to an array of complications:

(i) the ability of the multiple-scattering theory to convert to single elastic scattering for small step sizes, thereby allowing multiple scattering steps to become arbitrarily small in the proximity of boundaries;

(ii) the design of the electron step algorithm that allows the same;

(iii) the energy loss evaluation over steps of varying length;

(iv) the correct implementation of path length corrections.

Nowadays, there are several codes that have been proven highly accurate in their handling of these effects, including EGSnrc (Kawrakow 2000) and PENELOPE (Salvat et al. 2001).

3.2 The Fano Test

The correct simulation of dosimeters, and specifically gas-filled ionization chambers, is one of the most stringent tests of a condensed history Monte Carlo code. Accurate chamber calculations require both the electron transport physics as well as the cross sections to be accurate. In the early days, the ability of Monte Carlo to calculate chamber response accurately was assessed by comparing the results to Spencer-Attix cavity theory (Rogers 1993), a result that was believed to be accurate for air-filled graphite chambers to within a few tenths of a percent at ^{60}Co. However, comparison against cavity theory tests both the consistency of the code as well as the accuracy of the cavity theory. The most accurate test of the inherent electron transport consistency irrespective of the accuracy of the cross sections is the so-called "Fano test." The Fano theorem states that *in conditions of charged particle equilibrium, the electron fluence in a medium is independent of density variations from point to point*. This feature can be used to test the extent to which the electron step algorithm, boundary crossing algorithm, and energy loss evaluation has been implemented adequately, and passage of this test is a mandatory requirement for Monte Carlo results in realistic situations to be trustworthy.

The Fano test is usually carried out on a cavity filled with the gaseous form of the phantom material in which the cavity is embedded. The idea is that the gaseous form of the wall material has exactly the same cross sections as the wall material itself but has a 1000-fold lower density. This means that density effects in gas and wall must be taken as the same. There are two flavors of the test, differing in the way CPE is established. One way is to start from a photon field, let it interact in the phantom (or wall) of the ionization chamber, and either restore the primary photon once it has interacted, discard the scattered photon, and follow the secondary electron slowing down (the regeneration technique) or, alternatively, by dividing the cavity dose by A_{wall}, the wall correction factor which eliminates the effects of attenuation and scatter, (or multiplying by K_{wall}). The Fano test now entails the comparison of collision kerma in the wall, under CPE with dose to the cavity, as follows:

$$D_{\text{cav}}^{\text{unw}} \equiv \frac{D_{\text{cav}}}{A_{wall}} = \left(\overline{\frac{\mu_{tr}}{\rho}}\right)_{wall} \left(1 - g_{wall}\right) \bar{E}\phi, \tag{5.7}$$

where ϕ is the primary photon fluence and E the photon energy. This technique was used by several authors during the investigation of accuracy of the EGSnrc (Kawrakow 2000; Seuntjens et al. 2002), the PENELOPE code (Yi et al. 2006), and GEANT4 (Poon et al. 2005). In equation (5.7), the quantities, $\left(\overline{\mu_{tr}}/\rho\right)_{wall}$ and g_{wall} are calculated in auxiliary calculations but should be based on the same interaction data as used in the cavity dose calculation.

A second way, that avoids these auxiliary calculations, is to realize Fano conditions by directly initiating an electron fluence with uniform intensity per unit mass in an infinite medium with a gap of infinite lateral extent. In this case the dose deposited in the gap or the wall is just the energy of the electrons times the number initiated per unit mass. Sempau and Andreo (2006) used this method to compare dose calculations with the condensed history Monte Carlo simulations with event-by-event calculations and arrived at a consistency of 0.2% with PENELOPE.

4. Reducing Variance

In the calculation of correction factors in measurement dosimetry, we generally deal with very small effects ("perturbations") on existing detector response models (e.g., the Spencer-Attix cavity theory). For example, wall corrections of ionization chambers are small since the walls of chambers are thin and made of low-Z materials having very similar interaction coefficients as the medium in which the chamber is placed. It is therefore impractical to gain sufficient statistics for calculating these effects just by doing straightforward calculations.

To briefly discuss the variance reduction techniques used these days, it is necessary to define efficiency. Efficiency for the Monte Carlo calculation of a quantity is defined as:

$$\epsilon = \frac{1}{s^2 T}, \tag{5.8}$$

where T represents the CPU time to obtain a value of s^2 which is an estimator of the variance σ^2 on the quantity of interest. Proper variance reduction techniques in Monte Carlo transport are defined as statistical methods or "tricks" that improve the efficiency of a Monte Carlo calculation by reducing the variance without affecting the physics, i.e., without introducing any approximations and thus maintaining the same expectation value for any quantity being scored. We discuss below the most important variance reduction techniques used in the context of the calculation of ionization chamber correction factors. There are also techniques that improve the efficiency by shortening the time to do the calculation for a given history, usually by introducing some approximation. In this case one must establish that any approximation does not lead to a change in the results.

4.1 Fluence-based Estimators

In this category quantities are scored (often "on-the-fly") directly from the fluence of the particles passing through a given volume element (voxel). The efficiency increase stems from the fact that it is not necessary for the particles to interact in the region of interest; they just have to pass through the region for the quantity to be scored. This technique is especially useful for low-energy photon simulations where one can score the dose using the kerma approximation via $\Psi(\mu_{en}/\rho)$ where Ψ is the energy fluence in a given region rather than scoring energy deposition only when the photons interact in a volume.

4.2 Correlated Sampling

Correlated sampling is a true variance reduction technique of major importance for the study of correction factors that involve the effect of small changes in the geometry. Ma and Nahum (1993a) discussed the improvement in efficiency obtained by using correlated sampling in the calculation of dose ratios and used it in the calculation of central electrode effects of ionization chambers (Ma and Nahum 1993b) and other applications of detector perturbation effects. Correlated sampling exploits correlations between similar geometries to reduce the uncertainty on the ratio or difference of the calculated quantities and reduces the total time required to reach a given precision. In the Ma and Nahum implementation, it does so by following a primary history until the particle enters a region that is marked to change, at which point the history is split and continued for the two (or more) geometry options in parallel. The quantities that are calculated are highly correlated and even though the precision on the quantity in absolute terms is no better than for a single simulation, the ratio of the quantities for differential geometries is much more precise. Buckley et al. (2004) discuss their correlated sampling implementation for EGSnrc in the user code CSnrc. Figure 5-2 illustrates their method. The correlated sampling (CS) region is the region defined as the one that differs between geometry options. For example, the task could be to calculate the dose ratio in the small region when first filled with water and afterwards with air. In figure 5-2 Track A never enters the CS region and gets only calculated once. Track B hits the CS region and its portion outside into the CS region is tracked only once. At the point of entry into the CS region, the particle's characteristics and the random number generator state are saved. The tracking of the original particle continues through the CS region and outside until the shower (for the first geometry option) terminates. At that point, the saved particle and random number state from when the main history entered the CS region is retrieved, the CS material(s) is (are) switched to geometry option 2, and the split history is tracked through the CS geometry, again, until the complete shower ends. The saved particle and random number state at the entry of the CS region is retrieved and transported for as many CS geometry options as present in the simulation.

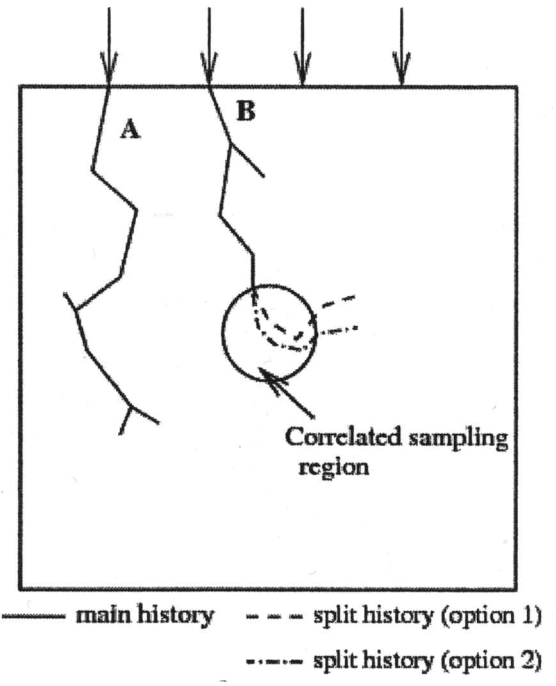

Figure 5-2. Illustration of the correlated sampling transport. [Reproduced from Buckley et al. (2004) with permission from American Association of Physicists in Medicine.]

Efficiency improvements in the CS method are obtained from (1) simulating many histories only once for multiple CS geometry options, (2) simulating the main history only once up to the point where the particle enters the CS region but, most importantly, (3) the strongly reduced uncertainties on the ratio or difference of quantities scored in the CS region. Buckley et al. (2004) quantify these gains by calculating relative uncertainties on the ratio of correlated quantities taking into account covariances. They found improvements ranging from a few percent to a factor over 60, depending on the specifics of a given calculation's geometry and how well the correlation between tracks is maintained in different materials.

4.3 Range Rejection

Charged particle (or loosely, electron) range rejection is an efficiency-improving technique in which the electron is eliminated if its residual range, potentially evaluated at each step, is such that it cannot reach the region of interest or escape from the current region. The approximation made is that radiative photons that might have been created and contributed to dose in the region of interest or escape the local region if the transport would have continued are not taken into account. Range rejection is therefore usually applied below a certain energy threshold where the

probability of such events can be ignored. A more rigorous approach can make range rejection into a true variance reduction technique. When the residual range is shorter than the distance to the region of interest, Russian Roulette is executed on these electrons with survival probability $1/n_r$ where $n_r > 1$, a user-defined integer number (i.e., if a random number $< 1/n_r$, the electron is continued with increased weight, $w_0 n_r$, otherwise it is discarded). Increased weight electrons (fat electrons) are able to create high weight (fat) photons, which need to be split n_r, times to avoid statistical fluctuations in the scoring region. Range rejection in the context of chamber calculations is usually used with the cavity of the ionization chamber as the target region.

4.4 Photon Splitting

Photon splitting is a variance reduction technique whereby a primary photon is split into n_s photons with weight w_0/n_s and the interaction sites of the split photons are made uniform along the direction of the primary photon. The scattered photons originating from each interaction site are killed with probability $1/n_s$. n_s can be selected to yield best efficiency. Kawrakow and Fippel (2000) used the photon splitting technique to speed up in-phantom dose calculations in voxel geometries by a factor of 5.

4.5 Photon Cross Section Enhancement

Using photon cross section enhancement (XCSE) the photon cross section of a material in an arbitrary region in the geometry is artificially increased by a factor b. Doing so, however, requires the subsequent transport to take into consideration weighting factors to adjust for this bias. This can be done as follows: In a region with cross section enhancement the incident photon will be split into an interacting portion (fraction $1/b$) and a non-interacting portion (fraction $1 - 1/b$). All particles originating from the interaction carry the weight w_0/b, where w_0 is the weight of the original photon. Out of these particles all electrons are further transported but all photons (including relaxation photons, bremsstrahlung, and annihilation photons from subsequent electron transport) are terminated with probability $1/b$ so that, if they survive, they again have the original weight w_0. The unscattered portion of the incident photon is also terminated via Russian Roulette with probability $1 - 1/b$ making the weight of survivors w_0. In this way all electrons set in motion in the CSE region carry the weight w_0/b and there are b times more such electrons compared to transport without cross section enhancement.

One problem with the technique is that if an electron that was set in motion outside the CSE scoring region enters that region, it will have a weight of w_0 and therefore affect the statistical fluctuations. There are different ways to avoid this situation. First, one could simply surround the CSE scoring region, with at least one shell of CSE-enhanced region of thickness slightly larger than the maximum electron range so that no fat electrons can make it through into the volume of interest. A

more elegant and safer approach is to equalize the weights of electrons moving into the region of interest (Wulff et al. 2008). When an electron leaves a region with CSE factor b_1 to move into a region with CSE factor b_2, where $b_2 > b_1$, the electron is split into b_2/b_1 copies each with weight $w_0 b_1/ b_2$. If $b_2 < b_1$ then Russian roulette is played with survival probability b_2/b_1 (i.e., if (random number < b_2/b_1) the electron survives) and the weight of the surviving electron is set to $w_0 b_1/ b_2$.

4.6 Other Methods

The methods discussed above are very useful in many types of dosimetry calculations. There are other types of variance reduction techniques that offer dramatic speed ups (factors of 10 to 10^5) for accelerator simulations such as Directional Bremsstrahlung Splitting (DBS) (Kawrakow et al. 2004) and Bremsstrahlung Cross Section Enhancement (BCSE) (Ali and Rogers 2007). Methods like these emphasize those histories which are most relevant to the problem at hand and minimize the time spent tracking histories which are not critical (such as those going away from the patient). For fast calculations of dose in phantom, the STOPS algorithm developed by Kawrakow (2001) is another example of a powerful variance reduction technique. This is a sophisticated way to reuse information about a track history.

5. Monte Carlo–Calculated Quantities Associated with Dosimeter Response

5.1 Stopping-Power Ratios

Perhaps, the most important early application of Monte Carlo techniques was the calculation of water to air stopping-power ratios (SPRs) for use in electron beam dosimetry. SPRs are essential for the conversion of ion chamber readings into dose to water. They vary strongly with depth in an electron beam due to the rapidly changing average energy of the electrons with depth.

The Spencer-Attix (SA) stopping-power ratio is defined as:

$$\left(\frac{\bar{L}}{\rho}\right)_g^m = \frac{\int_{\Delta}^{E_{max}} \left(\Phi_T\right)_m \left(L_\Delta/\rho\right)_m \, dT + T E_m}{\int_{\Delta}^{E_{max}} \left(\Phi_T\right)_m \left(L_\Delta/\rho\right)_g \, dT + T E_g}, \tag{5.9}$$

where Φ_T is the electron fluence spectrum in the medium at kinetic energy T, Δ is the low-energy threshold above which electrons are tracked and below which there is either CPE or electrons are considered at rest, $(L_\Delta/\rho)_m$ is the restricted mass collision stopping power of the medium, and TE is the so-called "track-end dose" accounting for the dose deposited by electrons whose kinetic energy falls below Δ.

Early calculations of stopping-power ratios consisted of a two-step approach which involved the precalculation of an electron fluence spectrum in a volume (or range of volumes) of interest in the medium and averaging the restricted collision stopping power over the electron fluence. The calculation of electron fluence spectra held some special consideration in scoring and binning. To score the fluence, one basically needs to sum the path-length per unit volume in each energy bin in each geometric region of interest. The energy scale is subdivided into bins and the path-length is distributed into the various electron energy bins during the process of slowing down. This can become somewhat complex to handle as the electron's energy may cross many energy bins in a single step.

The two-step technique has the disadvantage that the amount of data can be large if stopping-power ratios are needed at, for example, a large number of positions or in conditions of differential geometry. To calculate stopping-power ratios in different conditions more flexibly, use is often made of the so-called "on-the-fly" scoring technique. Using this technique the total dose deposited in the two different media is scored, as represented by the numerator and denominator in equation (5.9) but for a calculation in which the cavity is filled with the transport medium, not the detector medium. The energy deposition in a condensed history code can take four distinct forms:

1. Energy deposition over a step with initial and final energy above Δ.
2. Energy deposition over a step that initiates with energy above Δ and that crosses Δ.
3. Energy deposition by particles whose history is terminated because their energy has fallen below Δ.
4. Energy deposition by particles created with kinetic energy below Δ.

In the EGSnrc user-code SPRRZnrc, contribution 1 is evaluated by summing the energy deposited over the step for the medium in the numerator and summing the same energy deposition, scaled by the ratio of the restricted stopping powers cavity material to medium material, evaluated at the mid-point of the step. Contribution 4 is not scored at all (they are not part of the Spencer-Attix electron fluence, as they cannot cross the cavity). Contribution 3 is scored as part of the track-end term by summing its energy deposition in the numerator and the energy deposition, scaled by ratio of stopping power cavity material to medium material evaluated at Δ. Contribution 2 is considered in two parts: the part above Δ which is treated as a deposition event as in contribution 1, and the part below Δ, which is counted in the track-end term (contribution 3). The calculation of stopping-power ratios using the on-the-fly method is a comparatively efficient technique since the numerator and denominator dose calculations are highly correlated. Statistical uncertainties typically are easily below 0.1% without the application of special variance reduction techniques.

Stopping-power ratios have been calculated since the late 1970s (Berger et al. 1975; Nahum 1978) as part of reference dosimetry data and are the main component underlying the beam quality conversion factors k_Q and $k'_{R_{50}}$ (see chapter 9). Stopping-power ratios have also been calculated for relative dosimetry with air-filled chambers and other detectors (Wang and Rogers 2007) with the goal to convert depth ionization into depth dose in electron beams (Burns et al. 1996).

A first issue in the use of Spencer-Attix stopping-power ratios and their ability to accurately estimate detector response is the simplistic way in which detector geometry is specified. The Δ in the theory is conceptually not rigorously defined and is usually taken as the energy of an electron with a residual range in air equal to l, the mean chord length of electrons in the cavity of the ion chamber. For an isotropic electron field uniformly entering a convex cavity, $l = 4\ V/S$ where V is the volume and S is the surface area. This is the expression used by most standards laboratories to determine the value of Δ appropriate for their standard cavity chambers. However, electrons entering the cavity of an ion chamber are not necessarily isotropic, nor are all ion chambers convex. Rogers and Kawrakow (2003) compared the mathematical mean chord length to a Monte Carlo calculated mean chord length and found a negligible difference for cavity chambers used in standards laboratories. In protocol dosimetry a chamber-independent 10 keV is often used for a large variety of ionization chambers. In a study of systematic correction factors to the Spencer-Attix theory at low photon energies, Borg et al. (2000) showed that adequate choice of the Δ improves the accuracy of the Spencer-Attix cavity theory. A second issue and, in fact, important limitation of Spencer-Attix stopping-power ratios is that the cavity fluence is not evaluated and hence, important errors can be made by ignoring fluence perturbation corrections when stopping-power ratios are used to approximate dose ratios in regions of disequilibrium. An extreme example of this is given in figure 5-3 from Paskalev et al. (2002), where the ratio of average cavity dose to average dose to water for an Exradin A14P micro-parallel-plate ion chamber in a circular 1.5 mm diameter field is compared to the stopping-power ratio water to air for a similar field size and for a 10×10 cm^2 field size. For an ideal Spencer-Attix cavity these two quantities should be the same, but as pointed out in chapter 3, application of Spencer-Attix stopping-power ratios needs to go hand-in-hand with the capability of sampling the fluence at a representative position for the method to better approximate dose ratios for realistic detectors. However, these effects are traditionally handled by replacement corrections. Figure 5-3 demonstrates that these effects are very drastic for situations in which disequilibrium effects over the cavity volume are significant. This issue will be further discussed in section 5.7.

5.2 Mass-Energy Absorption and Mass-Energy Transfer Coefficient Ratios

The calculation of mass-energy absorption and mass-energy transfer coefficient ratios in the context of dosimeter response and in-air and in-phantom dose measure-

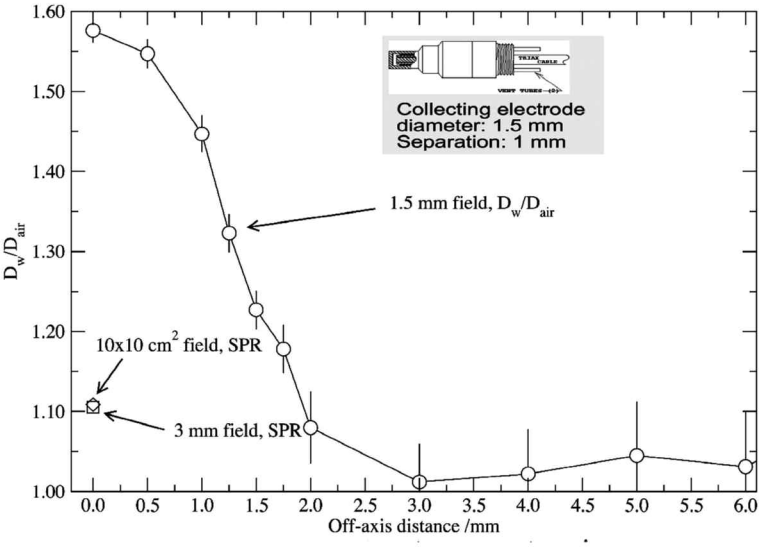

Figure 5-3. Ratio of average dose to water to dose to air in the cavity of an Exradin A14P ion chamber as a function of off-axis distance in one 1.5 mm diameter 10 MV field. [Data replotted from Paskalev et al. (2002) with permission from the author.]

ments has been addressed at length in the literature for high-energy photon beams (Cunningham et al. 1986; Furhang et al. 1995) and kilovoltage beams (Ma and Seuntjens 1999; Seuntjens et al. 1987, 1988). The data have been used to determine correction factors in the context of dosimetry protocols (IAEA 1987; AAPM TG–21 1983; IAEA 2000; Almond et al. 1999; Ma et al. 2001) and in the description of scaling and dose transfer procedures.

The ratio of average mass-energy absorption coefficients is defined as:

$$\left(\frac{\overline{\mu_{en}}}{\rho}\right)_{m_1}^{m_2} = \frac{\int \left(\mu_{en}/\rho\right)_{m_2} \Phi_{E,2}\left(E\right) E\, dE}{\int \left(\mu_{en}/\rho\right)_{m_1} \Phi_{E,1}\left(E\right) E\, dE}, \tag{5.10}$$

where $(\mu_{en}/\rho)_{m_1}$ represents the mass-energy absorption coefficient in medium 1 and $\Phi_{E,1}$ represents the photon fluence, differential in energy, in the same medium. Evaluation of these quantities thus requires (1) basic interaction data and (2) availability of the photon fluence spectrum. Hubbell (1982) and more recently Seltzer (1993) published systematic compilations of mass-energy absorption coefficients as a function of photon energy for elements and materials of dosimetric interest. Measured spectra or Monte Carlo–calculated fluence spectra have been used to average the data under different conditions. On-the-fly scoring techniques have also been used to calculate the average ratios simultaneously in different locations, thereby avoiding the intermediate storage of a large number of spectra.

5.3 In-Air Ionization Chamber Correction Factors

5.3.1 Wall Correction Factors

Wall correction factors in the context of air kerma or exposure measurements play an essential role in the process of determining air kerma from measurements using an ionization chamber with a wall and a known effective volume, or, in the process of determining the effective volume (or mass of air) in a chamber calibrated in a photon field with known air kerma. Bielajew (1986) formalized the role of wall correction factors in the context of a cavity theory for photon fields. Rogers et al. (1985) showed, at that time considered satisfactory, agreement to within 0.7% between measured and calculated A_{wall} factors. Measurements typically consisted of determining the response of the ion chambers with extra wall thickness added. The resulting response versus wall thickness plots are very linear and the standard method for determining the response for zero wall thickness was to extrapolate linearly to zero wall thickness and to make a small correction to account for the fact that electrons drift in the direction of the beam before depositing their energy. In subsequent years statistical uncertainties and consistency of the Monte Carlo–calculated wall correction factors improved and by 1990 it became clear that there were systematic differences between the correction as derived from the extrapolated response and the actual wall correction. Bielajew (1990) showed that this was not observed experimentally since the discrepancy was only apparent in the region where the lack of buildup in the wall also affected the response. Detailed experimental studies by McCaffrey et al. (2004) and Buermann et al. (2003) demonstrated the inaccuracy of the linear extrapolation technique and the accuracy of the Monte Carlo correction factors.

Wall corrections are calculated in a process of correlated scoring of:

1. the total energy deposition, i.e., all secondary electrons and their progeny from primary and scattered photons $\langle \epsilon \rangle = \langle \epsilon_0 + \epsilon_{\text{scat}} \rangle$, where $\langle \epsilon_{\text{scat}} \rangle$ is the energy deposition from all secondary electrons and their progeny produced by photons interacting in the chamber;

2. the "first-collision" energy deposition by all secondary electrons and their progeny from only primary photon interactions $\langle \epsilon_0 \rangle$; and

3. the "unattenuated first-collision" which is the first-collision energy deposition, corrected for attenuation of the primary photon $\langle \epsilon_0 e^{+\mu t} \rangle$ where t is the distance traveled in the chamber before interacting.

All scores are done simultaneously for each history making the scoring highly correlated, which greatly reduces the statistical uncertainty in the ratios. The wall correction is usually scored as a product of two factors, the attenuation correction and a scatter correction defined as:

$$K_{\text{at}} = \langle \varepsilon_0 e^{\{+\mu t\}} \varepsilon_0 \rangle \, / \, \langle \varepsilon_0 \rangle, \tag{5.11}$$

$$K_{\text{scat}} = \langle \varepsilon_0 \rangle / \langle \varepsilon_0 + \varepsilon_{\text{scat}} \rangle, \tag{5.12}$$

$$K_{wall} = K_{\text{at}} K_{\text{scat}} = \langle \varepsilon^{\{+\mu t\}} 0 \rangle / \langle \varepsilon_0 + \varepsilon_{\text{scat}} \rangle. \tag{5.13}$$

In equations (5-11) to (5-13), K_{scat} is the fractional contribution to the energy deposited in the cavity gas from primary photons, and K_{at} corrects for the attenuation of the primary photons. Figure 5-4 shows wall corrections calculated by Seltzer and Bergstrom (2003) based on this method for one of the National Institute for Standards and Technology (NIST) spherical chambers in a parallel beam of monoenergetic photons. Despite the fact that codes in the late 1980s/early 1990s such as EGS4/PRESTA were not able to calculate ionization chamber response to better than approximately 1% for chambers of low-Z materials, the scoring method outlined above is accurate to well below 0.1%. This is due to the fact that the 1% uncertainty in the cavity calculation due to errors in electron transport, boundary crossing, etc., contributes in roughly the same way to both the energy deposition and the attenuation-corrected energy deposition for attenuation in relatively thin, low-Z walls. Wall corrections derived by performing cavity dose calculations with regeneration (see section 3.2) also allow the determination of K_{wall} but may be more cumbersome if the calculations with and without regeneration are not done on-the-fly.

The variance reduction techniques usually used for the in-air calculations of wall correction factors were photon forcing, typically, up to two forced photon interactions, and range rejection with an energy threshold.

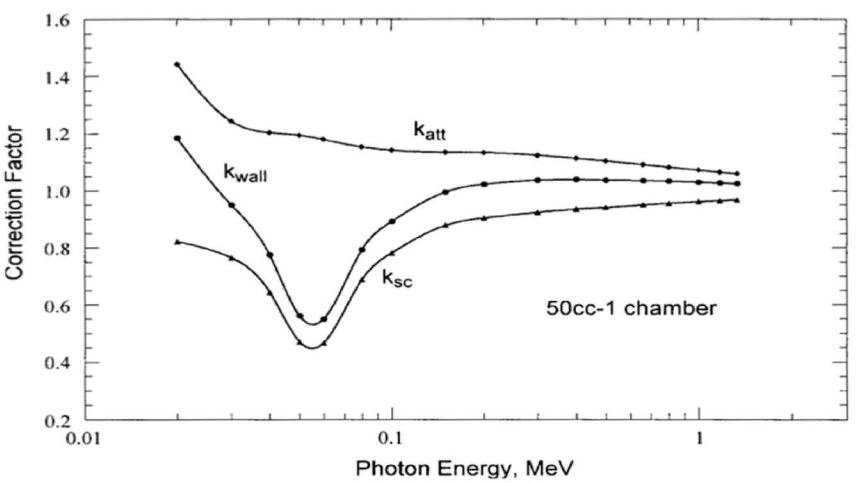

Figure 5-4. Components of the calculated wall correction for the NBS-NIST 50cc-1 spherical graphite standard chamber (wall thickness: 0.365 cm, ρ = 1.73 g/cm^3). The points are from Monte Carlo calculations for monoenergetic, parallel beams of photons; the curves are natural-cubic-spline fits to the data. Reproduced from data in Seltzer and Bergstrom (2003).

5.3.2 Other Quantities and Correction Factors

Equation (5.4) includes the correction for radiative loss g_m [for air as the medium in equation (5.4)], the average fraction of the kinetic energy of secondary charged particles (produced in all the types of interactions) that is subsequently lost in radiative (photon-emitting) energy-loss processes as the charged particles slow to rest in the medium. As part of the compilation on photon interaction coefficients, Seltzer (1993) developed expressions for g that include the radiation losses in elements and in mixtures of dosimetric importance. Monte Carlo techniques have also been used to calculate g (see appendix A). The calculation is typically in an infinite medium. Energy transfer after the first photon interaction (scattered photon eliminated) is scored as well as total energy of the photons created as a result of the radiative processes occurring during the slowing of the secondary charged particles.

There are a number of additional correction factors in equation (5.4) that can be expressed as ratios. The definition of these depends on how the air kerma is retrieved from the cavity dose once all the corrections are multiplied together. Typically, K_{an} corrects for the axial nonuniformity due to the point source nature of the beam instead of the photon beam being parallel; K_{comp} is a correction for the composite, i.e., nonuniform, nature of the wall material, if any, and other corrections for other non-ideal conditions, e.g., corrections for stems, central electrodes of different material from the wall, radial nonuniformity of the beam, etc.

5.4 In-Phantom Ionization Chamber Correction Factors In Conventional Clinical Reference Dosimetry

Equation (5.3) shows the components of chamber response in terms of absorbed dose. The correction factors involved in equation (5.3) have historically been determined using a variety of techniques. In codes of practice such as TG-51 and TRS-398, stopping-power ratios were based on Monte Carlo calculations using ICRU-37 (ICRU 1984) data and realistic accelerator beams. P_{wall} was based on a two-component model involving Monte Carlo stopping-power ratios and mass-energy absorption coefficient ratios, P_{cel} was based on correlated sampling dosimeter calculations by Ma and Nahum (1993b), and P_{repl} was based on seminal experimental work from Johansson et al. (1977). These different sources of data have led to some inconsistencies in definition of the correction factors.

Over the last half decade, significant progress has been made in in-phantom ionization chamber correction factor calculations made possible primarily by:

(i) Monte Carlo codes that are passing the Fano test at the 0.1% to 0.2% level,

(ii) the recent development of powerful variance reduction techniques and more realistic geometry specification,

(iii) the rapid increase in computing power relatively easily available.

5.4.1 Central Electrode Correction Factors

Ma and Nahum (1993b) used correlated sampling in EGS4 to calculate central electrode correction factors. Buckley et al. (2004) revisited central electrode corrections in photon and electron beams using correlated sampling dose calculations with EGSnrc. Figures 9-13 and 9-14 in chapter 9 show central electrode correction factors for an NE2571 cylindrical chamber in photon and electron beams. The reevaluation shows that the Ma and Nahum results adopted in TG-51 are accurate for photon beams except perhaps for the highest energy. The results for electron beams are slightly more variable. For graphite central electrodes at the lowest energy, the difference amounts to no more than 0.2%.

5.4.2 Wall Correction Factors

For wall correction factors associated with air-kerma standards and air-kerma–based reference dosimetry, due to the method used to calculate the factor, the calculation is relatively short and calculation accuracy had less impact on the accuracy. The situation is very different for wall corrections associated with in-phantom absorbed-dose measurements where electron transport accuracy is more critical and the calculation more CPU intensive. In this case, the wall corrections for ionization chambers have traditionally been handled approximately in dosimetry protocols. For cylindrical chambers in photon beams, the Almond and Svensson (1977) two-component model has been used where the effect of the wall *material* was estimated by considering the contribution to the cavity ionization from photons interacting in chamber wall versus the contribution of photons interacting in the phantom. Monte Carlo simulations of stopping-power ratios and mass-energy absorption coefficient ratios are combined with data from an experiment in which the ionization in a chamber was measured as the wall was gradually increased. This approach has led to inaccuracies on the order of 0.5% in the calculation of wall correction factors for chamber types with certain wall materials or thicknesses. The problem of accurate calculation of wall correction factors using the two-component model extends also to the effect of waterproofing sleeves for which the extended two-component model was shown to be problematic. In electron beams, wall corrections have traditionally been ignored. In early calculations using the correlated sampling method, Ma and Nahum (1994) used the EGS4 code to study wall and fluence perturbation correction factors for the NACP-02 chamber. In the last 3 years, a series of studies has appeared dealing rather definitively with wall correction factors in photon and electron beam reference dosimetry.

For photon beams, Buckley and Rogers (2006) studied P_{wall} correction factors obtained using correlated sampling implemented in the CSnrc user code. They validated their calculations by comparing their results to ratios of measurements of k_Q of chambers with close-to identical shape but differing in wall material and thickness and to measurements of ratios of the factor C_Q[1] for a chamber with various

[1] C_Q represents the ratio of the ^{60}Co absorbed dose calibration coefficient to the air-kerma calibration ^{60}Co coefficient, i.e., $C_Q = N_{D,w}^{^{60}Co} \Big/ N_K$. When measured, the absolute value of C_Q depends on both the air kerma and absorbed dose standard used; ratios of C_Q for different cap materials/thicknesses do not depend on these and only depend on the difference in build-up cap.

build-up caps of different materials and thicknesses to the C_Q value for a given build-up cap material. After validation, they compared their P_{wall} calculations to the Almond and Svensson formalism. Figure 9-18 in chapter 9 shows the ratio of the MC calculated wall correction factors and those derivred from the Svensson and Almond two-component model as implemented in TG-51.

Significant differences are observed especially for the wall materials containing A150 and graphite. By Monte Carlo–calculating all quantities involved in the two-component theory Buckley and Rogers also showed that these differences with the theory were due to limitations of the theory itself and not due to the underlying data: indeed, the theory only accounts for differences in material between wall and phantom material (water) and not for differences in the effect of scattering and attenuation in the wall.

The use of parallel plate chambers in photon dosimetry has traditionally been less well addressed. The reason for this is that parallel-plate chambers consist of more than a single material making up their walls and an extension of the two (or more) component model was not feasible. The exception to this are the experimental and Monte Carlo studies on wall correction factors in the context of absorbed dose to water calibrations in ^{60}Co beams. The significance of wall correction factors of parallel-plate chambers in absorbed-dose measurements in photon beams was established during the mid 1980s. EGS4-based Monte Carlo calculated P_{wall} correction factors were the basis of absorbed-dose beam quality conversion coefficients despite the known systematic uncertainties in the Monte Carlo codes at that time (see Almond et al. 1994 and references therein). More recently, however, Mainegra-Hing et al. (2003) used the EGSnrc code to revisit these calculations and calculated highly precise values of P_{wall} of 1.0207, 1.0048, and 1.0090 for the NACP-02, Markus, and Roos chambers, respectively. Buckley and Rogers (2006) revisited wall correction factors for parallel-plate chambers in high-energy photon beams and showed a relatively limited energy dependence of the wall correction for the NACP-02, Markus and Roos ionization chamber types (see figure 5-5).

In electron beams, the nature of the wall correction is quite different from that in photon beams and the main causes for wall corrections are backscattering from the back wall (or back portion of the wall) into the chamber and the effects of the extra density of the front wall. Experimental evidence and early MC calculations pointed to this effect quite clearly. Despite this, in current dosimetry protocols the wall correction factor has been assumed unity. Ma and Rogers (1995) and, more recently, Buckley and Rogers (2006a,b) used correlated sampling to calculate wall correction factors at the reference depth for electron beams with R_{50} ranging between 2 and 10.5 cm. They found that the wall correction factor at the reference depth decreases with energy and shows a fair amount of scatter when specified as a function of R_{50}. For cylindrical chambers the wall correction does not differ from unity by more than 0.6%, the largest effect being for the A150 and the graphite-walled chambers. For parallel-plate chambers the correction varies between 1.8% and 0.2% as a function of R_{50} for four different parallel-plate chamber types. Similar results for individual chambers were reported by Zink and Wulff (2008) and by Verhaegen et al. (2006).

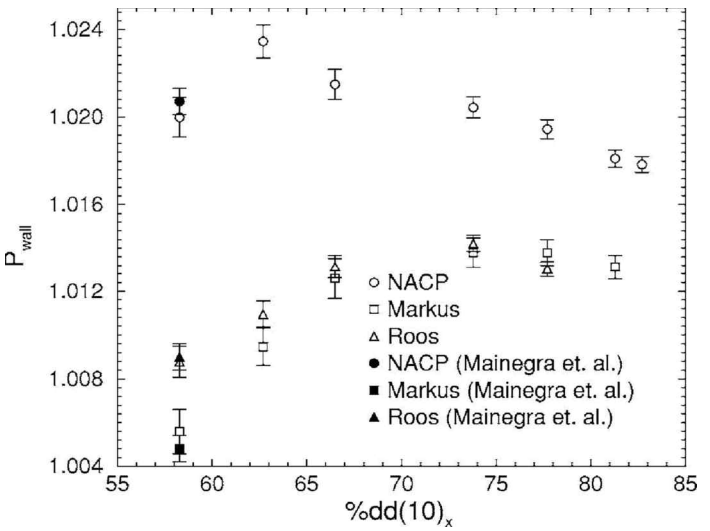

Figure 5-5. P_{wall} calculated using CSnrc as a function of photon energy. [Adapted from Buckley and Rogers (2006) with permission from American Association of Physicists in Medicine.]

5.4.3 Replacement Correction Factors

Replacement correction factors have been an important uncertainty component in reference dosimetry in external photon and electron beams for the last two decades and have been a source of confusion. They account for a compound effect consisting of dose gradient (in absence of the detector/chamber) and secondary electron fluence perturbation, related to the Bragg-Gray assumption that the electron fluence is unaffected by the presence of the cavity.

The replacement correction factor is often written as a product:

$$P_{repl} = P_{gr} P_{fl}, \tag{5.14}$$

where P_{gr} represents the gradient correction factor and P_{fl} the fluence perturbation correction factor (termed p_{dis} and p_{cav}, respectively in IAEA terminology). The gradient correction factor, which accounts for the fact that the dose distribution is not uniform, is often treated by moving the effective point of measurement to the depth (point) where one wants to measure the dose. The *effective point of measurement* is a concept that provides a link between average dose over the volume occupied by the cavity and dose *at a point*. If one assumes that the stopping power is approximately constant over the chamber cavity, the gradient effect represents the difference in integral electron fluence over the chamber cavity versus the value of the integral fluence at the point at which the dose is determined in the phantom. The fluence perturbation correction accounts for the change in the shape of the electron

fluence spectrum between these two situations. The overall effect of gradient and fluence perturbation, the replacement effect, cannot really be distinguished from the evaluation of the stopping-power ratio medium to cavity and its separation from the stopping-power ratio arises from historical reasons (the Bragg-Gray assumption).

The replacement correction factor has conventionally been handled differently for photon and electron beams. For photon beams, TG-51 (and TG-21) based its evaluation of these factors on the work by Cunningham and Sontag (1980) who studied the relative response of an ionization chamber inside a phantom cavity that was initially much larger than the chamber but that was progressively filled by putting build-up caps onto the chamber until the cavity around the chamber was completely filled. Using this approach, two effects are compounded, (1) scatter and attenuation in the (growing) wall and (2) the replacement effect. Replacement correction factors in TRS-398 (and TRS-277) were based on experimental data from Johansson et al. (1977) who used chambers of different sizes to measure the replacement effect. In electron beams, the gradient effect needs to be corrected for in an energy-specific and depth specific manner since the local gradient is not known *a priori*. Up until recently, the only reliable source for the determination of the fluence perturbation correction in electron beams were measurements relative to "well guarded" parallel-plate chambers in which it was assumed that the fluence perturbation correction factors could be ignored or, exceptionally, relative to other dose measurement techniques, such as Fricke dosimetry.

As part of a study of the complete perturbation effect in electron beams, Ma and Nahum (1994) studied P_{repl} values as a function of depth in electron beams. Verhaegen et al. (2006) calculated P_{fl} for the NACP-02 ionization chamber in 4 to 19 MeV electron beams of a calibration laboratory (NPL) and in 6 to 22 MeV clinical electron beams from a Varian CL2300 accelerator and found the factor to be about 1% below unity for all energies at d_{ref} and to increase with depth. Wang and Rogers (2008,2009) address the question of the replacement correction factor in high-energy photon and electron beams. They first established four methods to calculate the replacement correction factor, i.e., the stopping-power ratio method (SPR method); the fluence calculation method (FLU-method); the high-density air method (HDA-method, see figure 5-6) and the low-density water (LDW-method). In brief, the characteristics of these methods are as follows:

1. **SPR method:** The replacement correction is calculated as the ratio of the dose ratio, D_w/D_{air} and the Spencer-Attix stopping-power ratio, $\left(\bar{L}/\rho\right)_{air}^{w}$,

$$P_{repl}^{\text{SPR}}\left(Z\right)=\frac{D_w\left(z\right)}{D_{air}\left(\text{cavity}\right)}\Bigg/\left(\bar{L}/\rho\right)_{air}^{w}\left(z\right), \tag{5.15}$$

   where the stopping-power ratio is calculated separately, D_w is the dose in the phantom at the point of measurement, z, and D_{air} is the dose to the air in a wall-less cavity placed with its point of measurement at z.

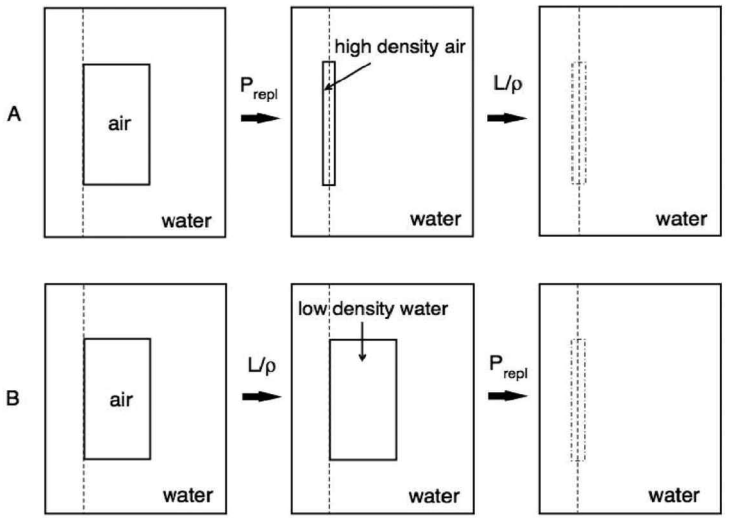

Figure 5-6. Schematic diagram illustrating the HDA (panel A) and LDW (panel B) techniques for the calculation of the P_{repl} factor for a schematic parallel-plate chamber. The effective point of measurement is chosen to be on the inner front surface of the chamber. [Adapted from Wang and Rogers (2008) with permission from American Association of Physicists in Medicine.]

2. **Fluence method:** The replacement correction is calculated as the ratio of total electron fluence, water to air:

$$P_{repl}^{\mathrm{FLU}}(z) = \frac{\Phi_w(z)}{\Phi_{air}(\mathrm{cavity})}. \tag{5.16}$$

3. **The high-density air (HDA) method:** The fluence correction is calculated as the ratio of the dose in a thin layer of air with water density, to the dose in the normal low-density air cavity:

$$P_{repl}^{\mathrm{HDA}}(z) = \frac{D_{\mathrm{HDA}}(z)}{D_{air}(\mathrm{cavity})}. \tag{5.17}$$

4. **The low-density water (LDW) method:** The fluence correction factor is calculated as the ratio of the dose in water at depth z to the dose in the cavity filled with low-density water:

$$P_{repl}^{\mathrm{LDW}}(z) = \frac{D_w(z)}{D_{\mathrm{LDW}}(\mathrm{cavity})}. \tag{5.18}$$

The SPR method requires a separate calculation of the stopping-power ratio water-to-air, which makes the P_{repl} calculation somewhat arbitrary. In the HDA method, the dose calculated in the high-density air layer depends on the thickness of the air layer and since there is only one value of the cavity air dose, the value of P_{repl} is not unique. Wang et al. (2009) studied the uncertainty associated with the choice of the thickness of the HDA slab and suggest that the slab should be chosen such that it is consistent with a Δ of a typical stopping-power ratio calculation of the chamber for which P_{repl} is to be calculated.

A typical Δ used in reference dosimetry protocols is 10 keV. The corresponding HDA thickness is on the order of 1.25 to 2.5 μm. Wang et al. showed that an HDA slab of this thickness is sufficiently thin so that the slab dose is not affected by fluence perturbation corrections. Based on the systematic uncertainty of selecting the appropriate slab thickness, an uncertainty on the order of 0.1% to 0.2% was assigned to the HDA method. A similar uncertainty estimate was made for the P_{repl} calculation using the LDW method. The different calculation methods were compared and demonstrated to be consistent with each other within the discussed uncertainties. Figure 5-7 shows the P_{repl} values as a function of depth for the NACP-02 chamber in a 6 MeV electron beam. Figure 5-8, from Wang (2009), presents the P_{repl} values for four frequently used parallel-plate chambers as a function of depth in water irradiated by a 6 MeV electron beam. This work demonstrates that (1) the correction factors in electron beams are strongly depth dependent; (2) the values for well-guarded chambers are not unity; (3) consistent with expectations and measurements, the values for the not well-guarded chamber (Markus) are much larger. Wang and Rogers (2008,2009) also calculated the replacement correction factors for a cylindrical chamber in ^{60}Co and found that the values were 0.5% less than those derived from the data of Cunningham and Sontag (1980). Their results for high-energy photon beams were compared to those based on measurements by Johansson et al. (1977) and showed that a normalization step performed in the analysis of the Johansson et al., data had led to an incorrect extraction of the P_{repl} values from that study. The experimental values used in the calculation of k_Q factors for both TG-51 (from Cunningham and Sontag 1980) and IAEA (from Johansson et al. 1977) were found to affect k_Q factors as shown in figure 9-25 of chapter 9. It is shown that the TRS-398 protocol overpredicts the relative effect at high energies by up to 0.6% for a Farmer chamber and the TG-51 protocol overpredicts by up to 0.2%. Wang and Rogers (2009) provide an empirical fit to their P_{repl} values for photon beams as a function of chamber radius and beam quality.

5.5 Absorbed-Dose Beam Quality Conversion Factors

Absorbed-dose beam quality conversion factors in the TG-51 protocol and the TRS-398 Code of Practice have been based on calculations of stopping-power ratios as a function of beam quality plus correction factors derived from a number of different experiments and models. In recent years a number of studies have presented direct Monte Carlo calculations of k_Q factors.

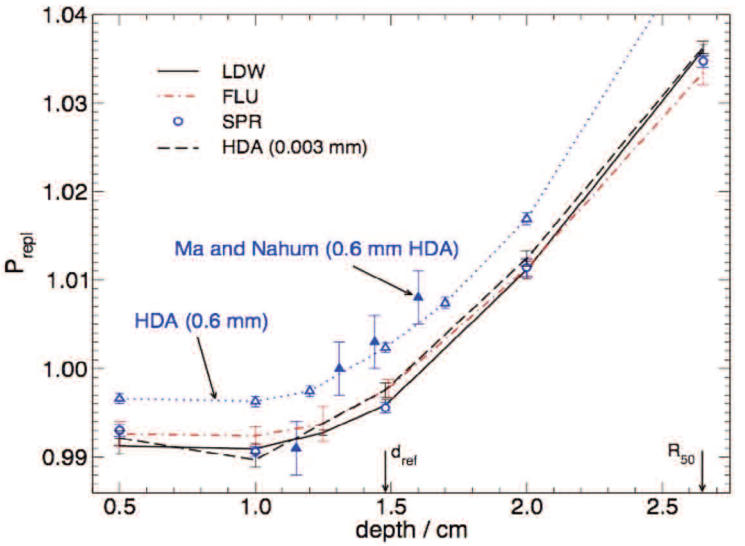

Figure 5-7. P_{repl} values calculated by the four techniques for the NACP-02 chamber as a function of depth in the 6 MeV electron beam. Values by Ma and Nahum calculated using a 0.6 mm HDA slab are also shown. [Reproduced from Wang and Rogers (2008) with permission from American Association of Physicists in Medicine.]

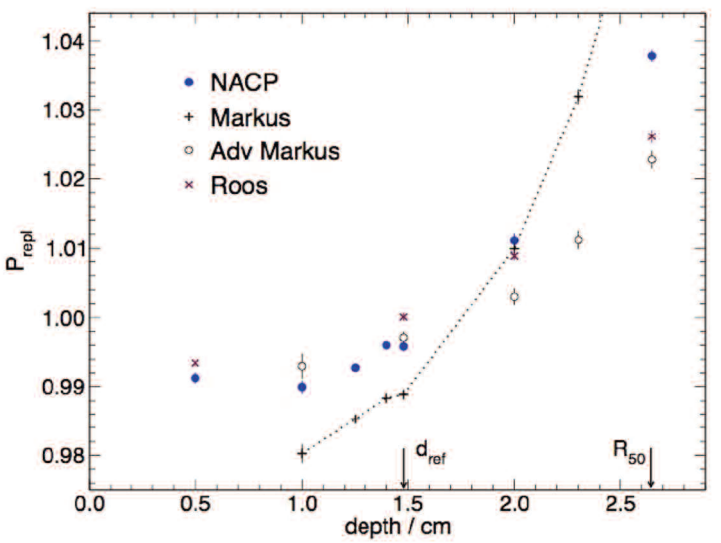

Figure 5-8. P_{repl} values calculated using the LDW method, for plane-parallel chambers as a function of depth in a 6 MeV electron beam. [Reprinted from Wang (2009); courtesy of L. Wang.]

Sempau et al. (2004) used PENELOPE (with correlated sampling and particle splitting) to calculate the overall conversion factor, D_w/D_{air}, i.e., the dose to water divided by the dose to the air in the cavity, a factor which is proportional to the k_Q factor. The calculations were for a realistic NACP chamber irradiated by electron beams at depth in water. They compared their results at d_{ref} as a function of beam quality specified by R_{50}, normalized to the value of the overall correction factor in the TRS-398 Code of Practice at 8.75 cm, to the values of the Code of Practice at lower values of R_{50}. With this normalization the authors found good agreement. The authors also presented calculations for the Wellhöfer PPC-40 and PPC-05 chambers and found the normalized conversion factors agree well with the TRS-398 data for the Roos chamber, which suggests that the chamber-dependent correction factors for the various chambers do not play a big role, or at least they are all the same.

Zink and Wulff (2008) used EGSnrc to calculate the response of the Roos parallel-plate chamber. The authors calculated the perturbation corrections P_{repl} and P_{wall} (p_{cav} and p_{wall}) for different electron energies and for ^{60}Co. Consistent with Buckley and Rogers, they also found that the wall correction factor P_{wall} depends on electron energy and decreases with increasing electron energy. For the lowest electron energies in their study ($R_{50} \approx 2$ cm), P_{wall} deviated from unity by up to 1.5%.

Figure 5-9 shows the stopping-power ratio water to air and the overall correction factor for a Roos chamber type as a function of R_{50}. These data indicate that there is a significant difference between direct calculation of the dose ratio and stopping-power ratio if the data are not normalized. The agreement improves if the data are normalized at the highest energy, but a discrepancy on the order of 1% remains at low energies.

Zink and Wulff also calculated the k_Q factor for the Roos chamber by also evaluating the wall and replacement correction factors at ^{60}Co energies. For electron energies $E_0 > 9$ MeV ($R_{50} > 4$ cm), their calculated values of k_Q were in good agreement with the TRS-398 values. Deviations in the range of 0.5% to 0.8% were found for $R_{50} < 3$ cm.

5.6 Relative Dosimetry in Conventional Beam Configurations and the Build-up Region

In the recent studies of ionization chamber correction factors, attention has been spent on the reevaluation of quantities at the reference depth. Some studies also presented data of correction factors at depths different from the reference depth. The goal of this is to provide depth-dependent correction factors that affect the accuracy of the measurement of relative dose. In the studies by Buckley and Rogers (2006a,b) and by Wang (2009) correction factors at multiple depths were presented. These depth dependencies can be substantial as shown in, e.g., figures 5-7 and 5-8. These variations in corrections with depth may affect, for example, the measured R_{50} values (Verhaegen et al. 2006). Recent powerful improvements in variance reduction techniques have enabled calculation of individual perturbation effects as a function of position (Wulff et al. 2008).

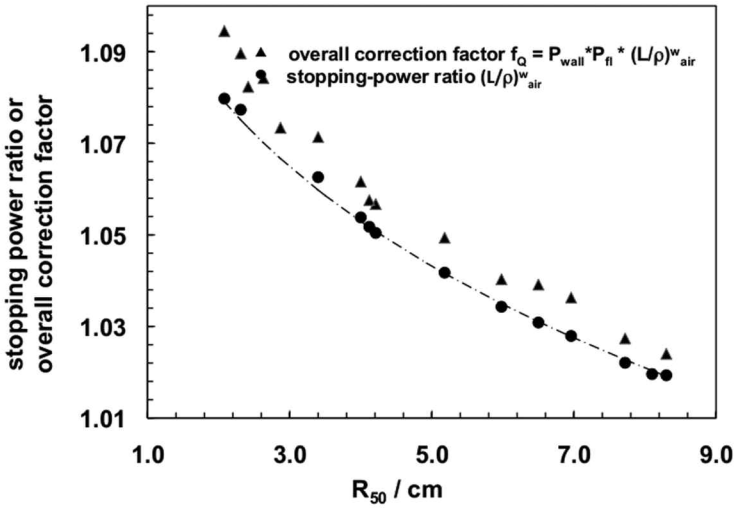

Figure 5-9. Restricted collision stopping-power ratios (proportional to the k_Q factor in the IAEA TRS-398 Code of Practice) and overall conversion factor calculated for the Roos parallel-plate chamber. (Reprinted from *Physics in Medicine and Biology,* "Monte Carlo calculations of beam quality correction factors k_Q for electron dosimetry with a parallel-plate Roos chamber." K. Zink and J, Wulff, vol 53, pp. 1595–1607. © 2008 with permission from IOP Publishing.)

In relative dosimetry it is not really clear how to deal with position-dependent correction factors. The above-mentioned studies give some means of correcting measured relative doses and one could envision chamber type dependent fits of the different correction factors as a function of position. However, for relative dosimetry this may be not practical: the correction factors are large in the build-up region and ionization chamber measurements have been challenging for practical and fundamental reasons. Another approach is to express the difference between relative dose and relative ionization as a shift in the point of measurement. Such a conglomerated approach has been proposed by Kawrakow (2006) who showed that the $0.6r$ upstream effective point of measurement (EPOM) shift adopted in the conventional protocols for photon beams to account for the corrections is incorrect and that the shift depends on every detail of the chamber design (i.e., cavity length and radius, mass density of the wall material, size of the central electrode), the beam quality, and the field size. Kawrakow's modified point of measurement shift for a PTW 233642 chamber was $-0.5r + 0.244$ mm and for an NE2571 $-0.6r + 0.335$ mm. In a set of highly accurate measurements, McEwen et al. (2008) confirmed Kawrakow's result and showed that the residual error after a $0.6r$ shift was generally around 0.5 mm (exceptionally up to 1.4 mm) for a wide range of ionization chambers. A comparison between measurements and Monte Carlo simulations showed that once (a) the correct EPOM is used, (b) the details of the linac geometry are correct, and (c) the parameters of the electron beam striking the bremsstrahlung

target have been adequately determined, Kawrakow's Monte Carlo calculations were capable of reproducing the experimental data to 0.2 mm or better. McEwen et al. (2008) provided the experimental EPOM shifts indicated in table 5-1 as measured relative to the NE2571 ionization chamber. Given the excellent agreement between experimental and Monte Carlo–calculated EPOM shifts, one could realistically envision tables with EPOM shifts to become part of clinical dosimetry protocols with the goal to provide enhanced accuracy for model-based treatment planning system commissioning. For parallel-plate chambers, both the Abdel-Rahman et al. (2005) and the McEwen et al. (2008) studies found that the highest accuracy depth-dose curves in megavoltage photon beams could be determined using a well-guarded parallel-plate ion chamber for which the thickness of the front window was scaled to water-equivalent depth as recommended in, for example, TRS-398 (IAEA 2000).

The impact of Monte Carlo simulations on the practice of build-up dose measurements has been taken one step further in a recent study by Ververs et al. (2009) where the authors devised a method to reduce the setup error inherent in clinical depth-dose measurements. The method was based on a detailed Monte Carlo simulation of the inflection region and minimization of the difference between measured and calculated percent-depth ionization (PDI) curve from which

Table 5-1. Shift in Effective Point of Measurement Relative to the NE2571 Chamber

All data were shifted by the default $0.6r$ upstream. The table indicates the additional shifts to apply to the chambers in order to achieve agreement with the NE2571 data. Positive shifts indicate moving the chamber downstream, towards the center of the chamber. The "air gap" represents the radial distance between the inside of the outer electrode and the outside of the inner electrode.

	Shift (mm)	Wall Thickness (g/cm^{-2})	Air Gap* (mm)	Electrode Diameter (mm)
NE2571	0	0.064	2.64	1
NE2581	0.18	0.040	1.64	3
PTW30001	0.20	0.045	2.55	1
PTW30013	0.10	0.056	2.55	1
Exradin A12	–0.06	0.088	2.55	1
Capintec PR-06G	0.23	0.050	2.70	1
NE2561/NE2611	0.33	0.090	2.70	2
PTW233642	–0.02	0.078	2.25	1
Exradin A16	–0.02	0.088	1.05	1

[Reproduced from McEwen et al. (2008) with permission from American Association of Physicists in Medicine.]

detailed ionization chamber positioning information can be extracted, *a posteriori*. The method was found to be robust with respect to sensitivity to beam related parameters (beam quality, field size, etc.).

5.7 Monte Carlo Techniques in Nonstandard Beam Dosimetry

Relative dosimetry in the build-up region is just one example of a clinically challenging measurement condition. The recent expansion of delivery technologies that use small fields or combinations of small fields composed in a dynamic fashion has presented new questions in dosimetry using ionization chambers. A new proposal for reference dosimetry in these fields was published by an IAEA committee of consultants (Alfonso et al. 2008), summarized in chapter 19. The dosimetric issues with these new technologies are twofold: (1) delivery technologies are unable to provide conventional reference fields but provide smaller fields instead which may distort electronic equilibrium and detector correction factors are thus required for accurate reference dosimetry; (2) delivery technologies often provide dynamic fields composed of small static fields. Several studies have shown that partial irradiation of chambers may lead to major dose measurement errors (Bouchard and Seuntjens 2004; Capote et al. 2004). The reason for these errors is the fact that the effective point of measurement becomes dependent on the delivery and somewhat unpredictable. A clinically acceptable solution would be to define a dynamic reference field in which charged particle equilibrium is theoretically reconstituted so that chamber corrections are minor and more easily predicted. Monte Carlo studies in such fields help quantifying the main residual corrections and studies by several groups are ongoing along these lines.

6. Summary and Outlook

This chapter summarizes the role that Monte Carlo simulations have played in the improvement of measurement dosimetry using ionization chambers. These range from the relatively simple calculations of mass-energy absorption coefficient ratios to detailed simulations of ionization chamber correction factors. To make this possible, both accuracy and precision needed to be improved. Compared to the early years when chamber-related factors were studied using Monte Carlo calculations, codes such as PENELOPE and EGSnrc have drastically improved and now pass the cross section independent Fano test at the 0.1% to 0.2% level. In addition, the cross sections themselves in the codes have become more accurate both in terms of relative distribution as well as in absolute terms. Furthermore, geometry specification has become much more accurate. Finally, powerful variance reduction techniques and concurrent powerful computer technology enable correction factor calculations at the sub 0.1% level, and this simultaneously at different locations in a measurement setup (see, e.g., Wulff et al. 2008).

The applications of these highly improved Monte Carlo calculations are endless. The measurement conditions discussed in this paper and addressed by the

majority of papers so far are limited to homogeneous static phantoms and relatively well-behaved beam conditions. Due to the more complex deliveries used routinely, the international community is now focusing on dosimetry of nonstandard and small beam configurations both in relative and absolute terms. One of the challenging issues in these situations is the number of degrees of freedom in irradiation conditions these delivery technologies bring with them.

The powerful impact of the direct Monte Carlo calculation of chamber dose, which is presumed to be proportional to chamber signal, enables the development of techniques to standardize complex dynamic deliveries as the traditional need to convert chamber signal to absorbed dose to water at a point diminishes and, in fact, has become a major source of uncertainty. The ideal solution of commissioning and verification of computerized treatment planning dose calculations can therefore be expected to incorporate the simulation of the measuring device with which the system is calibrated or verified. Getting to this point, however, will probably require intermediate steps to define delivery conditions that are more forgiving with respect to measurements such as proposed by Alfonso et al. (2008).

One can further envision that more complex clinical measurement conditions can be better modeled and better understood such as measurements in heterogeneous or in dynamic 4-D phantoms. The level of detail while simulating ionization chambers can also be further improved through explicit simulation of the electric field configurations, cable effects, and ionic recombination. These developments will help further reduce measurement uncertainties and improve clinical consistency.

References

Abdel-Rahman, W., J. Seuntjens, F. Verhaegen, F. Deblois, and E. B. Podgorsak. (2005). "Validation of Monte Carlo calculated surface dose for megavoltage photon beams." *Med Phys* 32:286–298.

Alfonso, R., P. Andreo, R. Capote, M. S. Huq, W. Kilby, P. Kjall, T. R. Mackie, H. Pal, K. Rosser, J. Seuntjens, W. Ullrich, and S. Vatnitsky. (2008). "A new formalism for reference dosimetry of small and nonstandard fields." *Med Phys* 35:5179–5186 .

Ali, E. S. M., and D. W. O. Rogers. (2007). "Efficiency improvements of x-ray simulations in EGSnrc user-codes using bremsstrahlung cross section enhancement (BCSE)." *Med Phys* 34:2143–2154.

Almond, P. R., and H. Svensson. (1977). "Ionization chamber dosimetry for photon and electron beams." *Acta Radiol Ther Phys Biol* 16:177–186.

Almond, P. R., P. J. Biggs, B. M. Coursey, W. F. Hanson, M. S. Huq, R. Nath, and D. W. O. Rogers. (1999). "AAPM's TG–51 protocol for clinical reference dosimetry of high-energy photon and electron beams." *Med Phys* 26:1847–1870. Also available as AAPM Report No. 67.

Almond, P. R., F. H. Attix, S. Goetsch, L. J. Humphries, H. Kubo, R. Nath, and D. W. O. Rogers. (1994). "The calibration and use of plane-parallel ionization chambers for dosimetry of electron beams: An extension of the 1983 AAPM protocol. Report of AAPM 904 Radiation Therapy Committee Task Group 39." *Med Phys* 21:1251–1260.

Berger, M. J. "Monte Carlo Calculation of the penetration and diffusion of fast charged particles" in *Methods in Computational Physics.* B. Alder, S. Fernbach, and M. Rotenberg

(eds.). Vol 1. New York: Academic Press, pp. 135–215, 1963.
Berger, M. J., S. M. Seltzer, S. R. Domen, and P. J. Lamperti. "Stopping-power ratios for electron dosimetry with ionization chambers" in *Biomedical Dosimetry.* Vienna, Austria: IAEA, pp. 589–609, 1975.
Bielajew, A. F. (1990). "On the technique of extrapolation to obtain wall correction factors for ion chambers irradiated by photon beams." *Med Phys* 17:583–587.
Bielajew, A. F. (1986). "Ionisation cavity theory: A formal derivation of perturbation factors for thick-walled ion chambers in photon beams." *Phys Med Biol* 31:161–170.
Borg, J., I. Kawrakow, D. W. O. Rogers, and J. P. Seuntjens. (2000). "Monte Carlo study of Spencer-Attix cavity theory at photon energies at or above 100 keV." *Med Phys* 27: 1804–1813.
Bouchard, H., and J. Seuntjens. (2004). "Ionization chamber-based reference dosimetry of intensity modulated radiation beams." *Med Phys* 31:2453–2464.
Buckley, L. A., and D. W. O. Rogers. (2006). "Wall correction factors, P_{wall}, for parallel-plate ionization chambers." *Med Phys* 33:1788–1796.
Buckley, L. A., I. Kawrakow, and D. W. O. Rogers. (2004). "CSnrc: Correlated sampling Monte Carlo calculations using EGSnrc." *Med Phys* 31:3425–3435.
Buermann, L., H. M. Kramer, and I. Csete. (2003). "Results supporting calculated wall correction factors for cavity chambers." *Phys Med Biol* 48:3581–3594.
Burns, D. T., G. X. Ding, and D. W. O. Rogers. (1996). "R_{50} as a beam quality specifier for selecting stopping-power ratios and reference depths for electron dosimetry." *Med Phys* 23:383–388.
Capote, R., F. Sanchez-Doblado, A. Leal, J. I. Lagares, R. Arrans, and G. H. Hartmann. (2004). "An EGSnrc Monte Carlo study of the microionization chamber for reference dosimetry of narrow irregular IMRT beamlets." *Med Phys* 31:2416–2422.
Cunningham, J. R., and M. R. Sontag. (1980). "Displacement corrections used in absorbed dose determinations." *Med Phys* 7:672–676.
Cunningham, J. R., M. Woo, D. W. O. Rogers, and A. F. Bielajew. (1986). "The dependence of mass energy absorption coefficient ratios on beam size and depth in a phantom." *Med Phys* 13:496–502.
Furhang, E. E., C. S. Chui and M. Lovelock. (1995). "Mean mass energy absorption coefficient ratios for megavoltage x-ray beams." *Med Phys* 22 525–530
Hubbell, J. H. (1982). "Photon mass attenuation and energy-absorption coefficients from1 keV to 20 MeV." *Int J Appl Radiat Isot* 33:1269–1290.
IAEA (2000). Absorbed Dose Determination in External Beam Radiotherapy: An International Code of Practice for Dosimetry Based on Standards of Absorbed Dose to Water. Technical Report Series TRS-398. Vienna, Austria: IAEA.
IAEA (1987). International Atomic Energy Agency. Absorbed Dose Determination in Photon and Electron Beams; An International Code of Practice. Technical Report Series TRS-277. Vienna, Austria: IAEA.
ICRU (1984). International Commission on Radiation Units and Measurements. ICRU Report 37. Stopping Powers for Electrons and Positrons. Bethesda, MD: ICRU.
Johansson, K. A., L. O. Mattsson. L. Lindborg, and H. Svensson. (1977). Absorbed-Dose Determination with Ionization Chambers in Electron and Photon Beams Having Energies Between 1 and 50 MeV. IAEA Symposium Proceedings. IAEA-SM-222/35 956. Vienna, Austria: IAEA, pp. 243–270.
Kawrakow, I. (2006). "On the effective point of measurement in megavoltage photon beams." *Med Phys* 33:1829–1839.

Kawrakow, I. "VMC++, Electron and Photon Monte Carlo Calculations Optimized for Radiation Treatment Planning" in *Advanced Monte Carlo for Radiation Physics, Particle Transport Simulation and Applications.* Proceedings of the Monte Carlo 2000 Meeting Lisbon, A. Kling, F. Barao, M. Nakagawa, L. T´avora, and P. Vaz (eds.). Berlin: Springer, pp. 229–236, 2001.

Kawrakow, I. (2000). "Accurate condensed history Monte Carlo simulation of electron transport. II. Application to ion chamber response simulations." *Med Phys* 27:499–513.

Kawrakow, I., and M. Fippel. (2000). "Investigation of variance reduction techniques for Monte Carlo photon dose calculation using XVMC." *Phys Med Biol* 45:2163–2184.

Kawrakow, I., D. W. O. Rogers, and B. Walters. (2004). "Large efficiency improvements in BEAMnrc using directional bremsstrahlung splitting." *Med Phys* 31:2883–2898.

Ma, C.-M., C. W. Coffey, L. A. DeWerd, C. Liu, R. Nath, S. M. Seltzer, and J. Seuntjens. (2001). "AAPM protocol for 40–300 kV x-ray beam dosimetry in radiotherapy and radiobiology." *Med Phys* 28:868–892. Also available as AAPM Report No. 76.

Ma, C.-M., and A. E. Nahum. "Plane-Parallel Chambers in Electron Beams: Monte Carlo Findings on Perturbation Correction Factor" in Proceedings of the IAEA International Symposium on Measurement Assurance in Dosimetry. Vienna, Austria: IAEA, pp. 481–493, 1994.

Ma, C.-M., and A. E. Nahum. (1993a). "Calculation of absorbed dose ratios using correlated Monte Carlo sampling." *Med Phys* 20:1189–1199.

Ma, C.-M., and A. E. Nahum. (1993b). "Effect of size and composition of central electrode on the response of cylindrical ionisation chambers in high-energy photon and electron beams." *Phys Med Biol* 38:267–290.

Ma, C.-M., and D. W. O. Rogers. (1995). "Monte Carlo calculated wall correction factors for plane-parallel chambers in high-energy electron beams." (Abstract). *Med Phys* 22:672.

Ma, C.-M., and J. P. Seuntjens. (1999). "Mass-energy absorption coefficient and backscatter factor ratios for kilovoltage x-ray beams." *Phys Med Biol* 44:131–143.

Mainegra-Hing, E., I. Kawrakow, and D. W. O. Rogers. (2003). "Calculations for plane-parallel ion chambers in ^{60}Co beams using the EGSnrc Monte Carlo code." *Med Phys* 30:179–189.

McCaffrey, J. P., E. Mainegra-Hing, I. Kawrakow, K. R. Shortt, and D. W. O. Rogers. (2004). "Evidence for using Monte Carlo calculated wall attenuation and scatter correction factors for three styles of graphite-walled ion chamber." *Phys Med Biol* 49:2491– 2501.

McEwen, M. R., I. Kawrakow, and C. K. Ross. (2008). "The effective point of measurement of ionization chambers and the build-up anomaly in MV x-ray beams." *Med Phys* 35: 950–958.

Nahum, A. E. (1978). "Water/air stopping-power ratios for megavoltage photon and electron beams." *Phys Med Biol* 23:24–38.

Paskalev, K. A., J. P. Seuntjens, and E. B. Podgorsak. "Dosimetry of Ultra-Small Photon Fields" in *Recent Developments in Accurate Radiation Dosimetry.* Proceedings of an International Workshop. J. P. Seuntjens and P. Mobit (eds.). Madison, WI: Medical Physics Publishing, pp. 298–318, 2002.

Poon, E., J. Seuntjens, and F. Verhaegen. (2005). "Consistency test of the electron transport algorithm in the GEANT4 Monte Carlo code." *Phys Med Biol* 50:681–694

Rogers, D. W. O. (1993). "How accurately can EGS4/PRESTA calculate ion chamber response?" *Med Phys* 20:319–323.

Rogers, D. W. O., and A. F. Bielajew. "Monte Carlo Techniques of Electron and Photon Transport for Radiation Dosimetry," in *The Dosimetry of Ionizing Radiation,* Vol III,

K. R. Kase, B. E. Bjärngard, and F. H. Attix (eds.). New York: Academic Press, pp. 427–539, 1990.

Rogers, D. W. O., A. F. Bielajew, and A. E. Nahum. (1985). "Ion chamber response and Awall wall correction factors in a ^{60}Co beam by Monte Carlo simulation." *Phys Med Biol* 30:429–443.

Rogers, D. W. O., and I. Kawrakow. (2003). "Monte Carlo calculated correction factors for primary standards of air kerma." *Med Phys* 30:521–532.

Salvat, F., M. Fernandez-Varea, E. Acosta, and J. Sempau. (2001). "PENELOPE: A Code System for Monte Carlo Simulation of Electron and Photon Transport Technical report, Nuclear Science Committee, Nuclear Energy Agency.

Sanchez-Doblado, F., P. Andreo, R. Capote, A. Leal, M. Perucha, R. Arrans, L. Nunez, E. Mainegra, J. I. Lagares, and E. Carrasco. (2003). "Ionization chamber dosimetry of small photon fields: A Monte Carlo study on stopping-power ratios for radiosurgery and IMRT beams." *Phys Med Biol* 48:2081–2099.

Seltzer, S. M. (1993). "Calculation of photon mass energy-transfer and mass energy absorption coefficients (dosimetry application)." *Radiat Res* 136:147–170.

Seltzer, S. M., and P. M. Bergstrom. (2003). "Changes in the U.S. primary standards for the air kerma from gamma-ray beams." *J Res Natl Inst Stand Technol* 108:337– 358.

Sempau, J., and P. Andreo. (2006). "Configuration of the electron transport algorithm of PENELOPE to simulate ion chambers." *Phys Med Biol* 51:3533–3548.

Sempau, J., P. Andreo, J. Aldana, J. Mazurier, and F. Salvat. (2004). "Electron beam quality correction factors for plane-parallel ionization chambers: Monte Carlo calculations using the PENELOPE system." *Phys Med Biol* 49:4427–4444.

Seuntjens, J., I. Kawrakow, J. Borg, F. Hobeila, and D. W. O. Rogers. "Calculated and Measured Air-Kerma Response of Ionization Chambers in Low and Medium Energy Photon Beams" in *Recent Developments in Accurate Radiation Dosimetry.* Proceedings of an International Workshop. J. P. Seuntjens and P. Mobit (eds.). Madison, WI: Medical Physics Publishing, pp. 69–84, 2002.

Seuntjens, J., H. Thierens, A. Van der Plaetsen, and O. Segaert. (1988). "Determination of absorbed dose to water with ionisation chambers calibrated in free air for medium energy X-rays." *Phys Med Biol* 33:1171–1185,

Seuntjens, J., H. Thierens, A. Van der Plaetsen, and O. Segaert. (1987). "Conversion factor f for X-ray beam qualities, specified by peak tube potential and HVL value." *Phys Med Biol* 32:595–603.

Verhaegen, F., R. Zakikhani, A. DuSautoy, H. Palmans, G. Bostock, D. Shipley, and J. Seuntjens. (2006). "Perturbation correction factors for the NACP-02 plane-parallel ionization chamber in water in high-energy electron beams." *Phys Med Biol* 51:1221–1235.

Ververs, J. D., M. J. Schaefer, I. Kawrakow. and J. V. Siebers. (2009). "A method to improve accuracy and precision of water surface identification for photon depth dose measurements." *Med Phys* 36:1410–1420.

Wang, L. L. W. (2009). Study of the Replacement Correction Factors for Ionization Chamber Dosimetry by Monte Carlo Simulation. Ph.D. Thesis, Carleton University, Ottawa, Ontario.

Wang, L. L. W., and D. W. O. Rogers. (2009). "The replacement correction factors for cylindrical chambers in high-energy photon beams." *Phys Med Biol* 54:1609–1620.

Wang, L. L. W., and D. W. O. Rogers. (2008). "Calculation of the replacement correction factors for ion chambers in megavoltage beams by Monte Carlo simulation." *Med Phys* 35:1747–1755.

Wang, L. L. W., and D. W. O. Rogers. (2007). "Monte Carlo study of Si diode response in electron beams." *Med Phys* 34:1734–1742.

Wang, L. L. W., D. J. La Russa, and D. W. O. Rogers. (2009). "Systematic uncertainties in the Monte Carlo calculation of ion chamber replacement correction factors." *Med Phys* 36:1785–1789.

Wulff, J., K. Zink, and I. Kawrakow. (2008). "Efficiency improvements for ion chamber calculations in high energy photon beams." *Med Phys* 35:1328–1336.

Yi, C. Y., S. H. Hah, and M. S. Yeom. (2006). "Monte Carlo calculation of the ionization chamber response to ^{60}Co beam using PENELOPE." *Med Phys* 33:1213–1221.

Zink, K., and J, Wulff. (2008). "Monte Carlo calculations of beam quality correction factors k_Q for electron dosimetry with a parallel-plate Roos chamber." *Phys Med Biol* 53: 1595–1607.

Problems

1. Equation (5.5) shows a possible set of definitions of ionization chamber correction factors P_{wall}, P_{cel}, and P_{stem}. Define an alternative possible set of definitions, equally acceptable, for wall, cel, and stem correction factors and discuss how your description differs from the one adopted in equation (5.5).

2. For a calculation of ionization chamber cavity dose, the standard deviation after 108 histories amounts to 1.5%.

   a. How many histories will it take to bring down the uncertainty to below 0.5%?

   b. How many histories would it take to achieve the 0.5% uncertainty if, through variance reduction, the efficiency were to be increased by a factor of 3?